Journal of Inorganic Biochemistry 259 (2024) 112643

Contents lists available at ScienceDirect

Journal of Inorganic Biochemistry

journal homepage: www.elsevier.com/locate/jinorgbio

Proton-triggered chemoselective halogenation of aliphatic C–H bonds with nonheme Fe^{IV}-oxo complexes

Neus Pagès-Vilà [a], Ilaria Gamba [a,b,*], Martin Clémancey [c], Jean-Marc Latour [c], Anna Company [a,*], Miquel Costas [a,*]

[a] Institut de Química Computacional i Catàlisi (IQCC), Departament de Química, Universitat de Girona, C/ Maria Aurèlia Capmany 69, 17003 Girona, Catalonia, Spain
[b] Departamento de Química, Facultad de Ciencias, Universidad de La Laguna, Av. Astrofísico Sánchez s/n, 38200 La Laguna, Spain
[c] Univ. Grenoble Alpes, CNRS, CEA, IRIG, Laboratoire de Chimie et Biologie des Métaux, F-38000 Grenoble, France

ARTICLE INFO

Keywords:
C–H halogenation
iron(IV)-oxo
Hydrogen atom transfer
Nonheme iron halogenases
Superacid changes chemoselectivity
Carbon-centered radical

ABSTRACT

Halogenation of aliphatic C–H bonds is a chemical transformation performed in nature by mononuclear nonheme iron dependent halogenases. The mechanism involves the formation of an iron(IV)-oxo-chloride species that abstracts the hydrogen atom from the reactive C–H bond to form a carbon-centered radical that selectively reacts with the bound chloride ligand, a process commonly referred to as halide rebound. The factors that determine the halide rebound, as opposed to the reaction with the incipient hydroxide ligand, are not clearly understood and examples of well-defined iron(IV)-oxo-halide compounds competent in C–H halogenation are scarce. In this work we have studied the reactivity of three well-defined iron(IV)-oxo complexes containing variants of the tetradentate 1-(2-pyridylmethyl)-1,4,7-triazacyclononane ligand (Pytacn). Interestingly, these compounds exhibit a change in their chemoselectivity towards the functionalization of C–H bonds under certain conditions: their reaction towards C–H bonds in the presence of a halide anionleads to exclusive oxygenation, while the addition of a superacid results in halogenation. Almost quantitative halogenation of ethylbenzene is observed when using the two systems with more sterically congested ligands and even the chlorination of strong C–H bonds such as those of cyclohexane is performed when a methyl group is present in the sixth position of the pyridine ring of the ligand. Mechanistic studies suggest that both reactions, oxygenation and halogenation, proceed through a common rate determining hydrogen atom transfer step and the presence of the acid dictates the fate of the resulting alkyl radical towards preferential halogenation over oxygenation.

1. Introduction

Halogenation of aliphatic C–H bonds is a relevant reaction in chemical synthesis and in biology because it introduces functionality into poorly reactive hydrocarbon skeletons. In nature, the reaction is performed by nonheme iron α-ketoglutarate (α-KG) dependent enzymes. Representative examples are CytC3 and SyrB2 [1,2]. The active site of these enzymes contains a mononuclear nonheme iron center and the crystal structure of SyrB2 has shown that it is bound to two histidines and a chloride atom [3].

The mechanism of reaction of these enzymes (Scheme 1) entails initial chelation of the α-KG cosubstrate through the α-carbonyl oxygen atom and a second oxygen atom of the anionic carboxylate group, triggering O_2 binding. O_2 activation follows the common mechanistic path of α-KG-dependent enzymes; in the case of SyrB2 and CytC3, a transient high spin $Fe^{IV}(O)$ species, generated after α-KG decarboxylation, has been detected and spectroscopically characterized, proposed to have a halide ligand in *cis* with respect to the terminal oxo unit [4,5]. These species have been kinetically proven to be the C–H cleaving agents. Halogenation of the aliphatic C–H bond is proposed to proceed via an initial hydrogen atom abstraction from the substrate by the terminal oxo ligand, affording an iron(III)-hydroxo-chloride intermediate and a carbon radical. The consequent rebound of the halide, instead of the incipient hydroxide ligand, to the carbon-centered radical affords the chlorinated product. The factors that determine halide instead of hydroxide ligand transfer in the natural systems have been a matter of discussion, and both experimental [6–8] and theoretical studies [9–15] have been pursued to understand the origin of this exquisite selectivity.

* Corresponding authors at: Institut de Química Computacional i Catàlisi (IQCC), Departament de Química, Universitat de Girona, C/ Maria Aurèlia Capmany 69, 17003 Girona, Catalonia, Spain.
E-mail addresses: ilgamba@ull.edu.es (I. Gamba), anna.company@udg.edu (A. Company), miquel.costas@udg.edu (M. Costas).

https://doi.org/10.1016/j.jinorgbio.2024.112643
Received 26 April 2024; Received in revised form 30 May 2024; Accepted 14 June 2024
Available online 17 June 2024

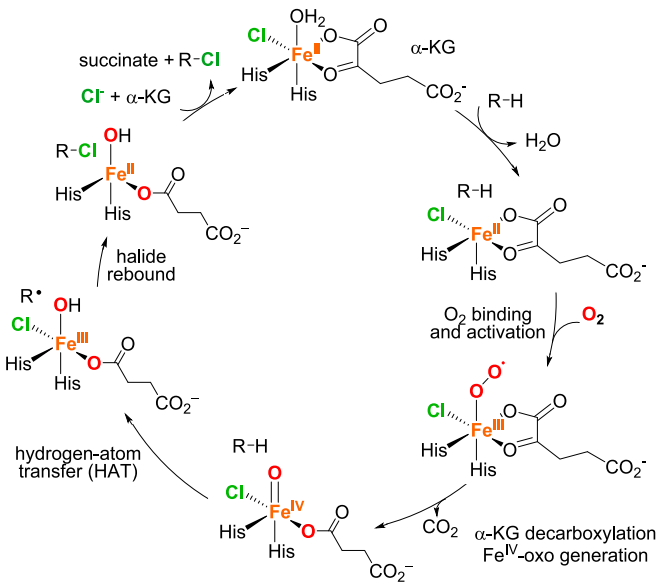

Scheme 1. General halogenation mechanism of nonheme iron dependent halogenases

Elegant studies by Krebs and Bollinger introducing mutations at the enzyme active site translated into perturbation of the halogenation versus hydroxylation chemoselectivity [16], strongly suggesting that halide transfer is favored by the specific positioning of the substrate carbon-centered radical that forms after hydrogen atom transfer (HAT) with respect to the reactive Fe^{III}–Cl bond.

In general terms, bioinspired or biomimetic studies rely on the preparation of small molecule model compounds that reproduce the structure or the reactivity observed in natural systems. They constitute an interesting strategy to get a better understanding of how natural systems work and to discover synthetically useful catalysts modelling the activity of enzymes [17,18]. Given the synthetic interest of C–H halogenation reactions, bioinspired complexes have been used as a tool to understand the origin of the unusual chemoselectivity exhibited by nonheme iron halogenases with the aim of designing catalysts performing the same transformation in an efficient manner. Recently, Goldberg and colleagues demonstrated that the selectivity of these small molecule models depends on the nature of the substrate radical. They prepared well-defined synthetic *cis*-Fe^{III}(OH)(X) species (X = Cl, Br) to model the critical rebound step in the natural systems. Reaction of these compounds with carbon-centered radicals showed the exclusive halide transfer to secondary carbon radicals as opposed to hydroxide transfer with tertiary carbon radicals, suggesting that bond strengths and reaction thermodynamics play a critical role in controlling the radical transfer selectivity [19,20].

The acquired knowledge regarding the origin of the selectivity of the halide rebound in halogenases may serve to design catalytic methodologies of utility in chemical synthesis. In this line, the stoichiometric halogenation of hydrocarbons by combining different oxidants and iron halide complexes has been documented in different cases [21–25], but direct detection of the C–H cleaving species could not be gained. Catalytic halogenation reactions have also been achieved with structurally related complexes using tetrabutyl ammonium salts as halide sources (either NBu_4Cl or NBu_4Br) albeit affording very modest turnover numbers [26,27]. In most of these examples, high-valent iron-oxo compounds have been postulated as the active species involved in the C–H halogenation on the basis of product analysis and computations, but direct evidence for such species could not be gained.

Well-defined iron(IV)-oxo-chloride complexes have been prepared and spectroscopically characterized in a small number of cases [28–31]. These compounds constitute structural models of the active species observed in mononuclear nonheme iron halogenases but reactivity studies have been described for only two of the reported examples. On the one hand, the ability of $[Fe^{IV}(O)(X)(^{Me,H}Pytacn)]^+$ (X = Cl and Br; Fig. 1) to break C–H bonds was proven, so that the initial HAT step could be modelled, but the resulting alkyl radical did not react with the Fe^{III}–Cl bond and no chlorination products were formed [30,32]. On the other hand, high spin (S = 2) $[Fe^{IV}(O)(X)(TQA)]^+$ complex (X = Cl and Br; Fig. 1) [31] reacted with cyclohexane and toluene under an argon atmosphere at −80 °C via a HAT reaction and it transferred the halide atom, producing the corresponding haloalkanes in 25–41% yields. The latter constitutes so far the only example of halogenation of aliphatic C–H bonds with a well-defined high valent iron-oxo-halide complex, thus modelling both the structure and reactivity of iron halogenases. Finally, C–H halogenation has also been accomplished with the well-defined iron(IV)-oxo compound $[Fe^{IV}(O)(2PyN2Q)]^{2+}$ (Fig. 1) in combination with a radical scavenger such as $CBrCl_3$ or with $[Fe^{II}(2PyN2Q)X]X$ (X = Cl, Br) [33]. In this particular case, the iron(IV)-oxo compound carries out HAT with cycloalkanes and alkylarenes, generating carbon-centered radicals that can be trapped by the radical scavenger or the iron(II)-halide complex producing the corresponding alkyl halides.

In this work we uncover the ability of well-defined iron(IV)-oxo complexes to change their chemoselectivity towards C–H bonds under certain conditions. Thus, we show that while the reaction of the iron (IV)-oxo species towards C–H bonds in the presence of an halide source affords only oxygenation products, the addition of a superacid to the reaction mixture results mainly in their halogenation. Mechanistic studies suggest that under both conditions the reaction occurs via a common HAT and the presence of the acid dictates the fate of the resulting alkyl radical towards preferential halogenation over oxygenation.

2. Results and discussion

2.1. Spin state of the starting iron(II) complexes

In this work we have selected a series of iron(II) complexes containing variants of the tetradentate N-based 1-(2-pyridylmethyl)-1,4,7-triazacyclononane (Pytacn) platform, which have been previously reported [34–36]. These are known to be suitable precursors for the preparation of the corresponding iron(IV)-oxo complexes [36,37]. We have chosen the substitution of the aliphatic nitrogens of the triazacyclononane by either a methyl (Me) or a neopentyl (Np) substituent, while a methyl group in the sixth position of the pyridine ring has been introduced in one case. The prepared ligands are ^{Np,H}Pytacn, ^{Me,Me}Pytacn and ^{Me,H}Pytacn and the corresponding iron(II) complexes have been prepared by equimolar reaction of the corresponding ligands with $[Fe^{II}(CF_3SO_3)_2(CH_3CN)_2]$ following the reported procedures (Fig. 2).

The iron centers in the synthesized complexes, $[Fe^{II}(CF_3SO_3)_2(^{Np,H}Pytacn)]$ (**1^{II}**), $[Fe^{II}(CF_3SO_3)_2(^{Me,Me}Pytacn)]$ (**2^{II}**) and $[Fe^{II}(CF_3SO_3)_2(^{Me,H}Pytacn)]$ (**3^{II}**), exhibit very similar geometric parameters according to their reported X-Ray structures [35,36,38]. The metal is hexacoordinate and the $^{R,R'}$Pytacn ligand wraps around the metal center leaving two free positions in a relative *cis* configuration that are occupied by the triflate counteranions in **1^{II}** and **3^{II}**. The same geometry is observed for **2^{II}**, but in this case it crystallizes with coordinated aqua ligands instead of triflate anions which act as non-bonding counteranions [39]. The Fe–N bond distances are around 2.2 Å, which are indicative of high spin ferrous centers. However, in acetonitrile solution, where triflate ions are replaced by acetonitrile ligands, differences among the three complexes arise. The ^{1}H NMR spectrum of **3^{II}** is typical of a low spin complex at 298 K, as evidenced by its compact NMR window (Fig. S1c) [35]. Instead, the ^{1}H NMR spectra of **1^{II}** and **2^{II}** at 298 K show spectral windows expanding from 140 to −40 ppm characteristic of paramagnetic molecules indicative of high spin Fe^{II} centers (Fig. S1a and S1b) [36,40]. Interestingly, the Mössbauer spectrum of **1^{II}** in acetonitrile at 80 K has been previously reported and it shows the

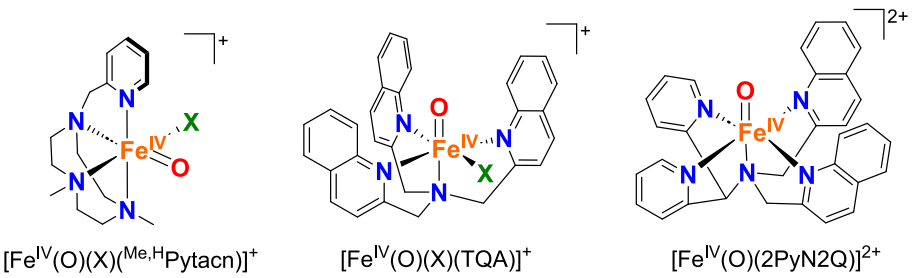

Fig. 1. Previously reported well-defined iron(IV)-oxo species as structural or functional models of nonheme iron halogenases.

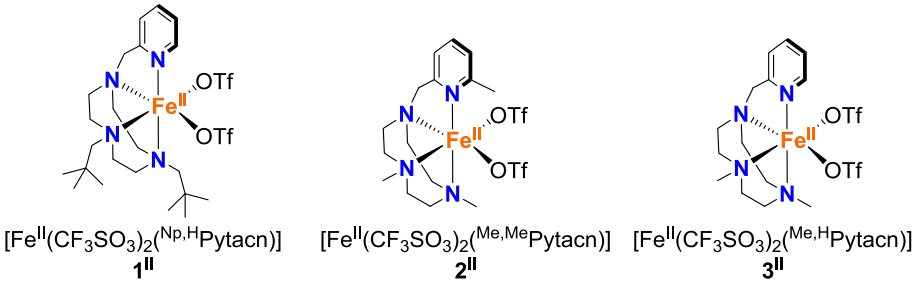

Fig. 2. Iron(II) complexes used in this work.

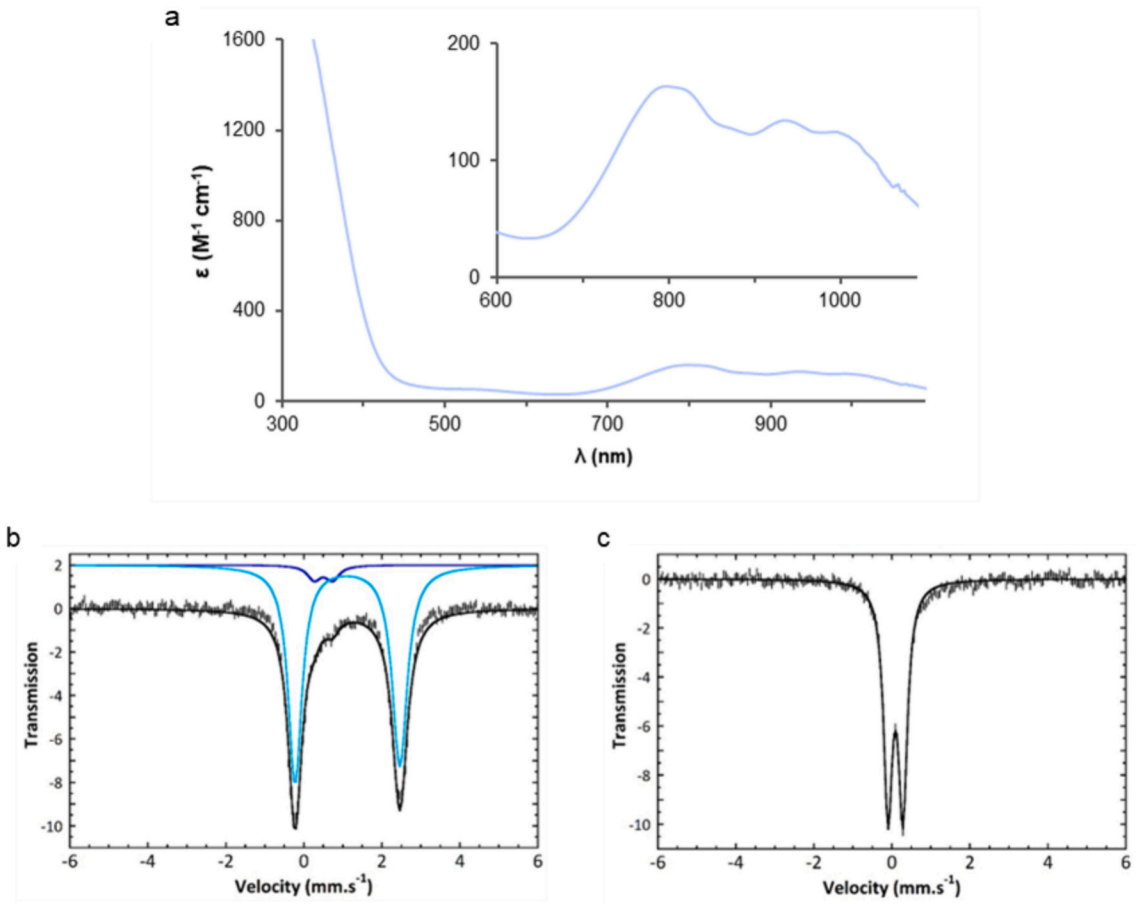

Fig. 3. a) UV–Vis spectrum of $\mathbf{2^{IV}(O)}$ recorded upon oxidation of $\mathbf{2^{II}}$ with 1 equiv. of Bu_4NIO_4 in the presence of 0.75 equiv. Tf_2NH in CH_3CN at −40 °C. **b)** Mössbauer spectrum of ^{57}Fe-enriched $\mathbf{2^{II}}$ recorded in acetonitrile at 80 K in the absence of magnetic field (vertical bars: experimental spectrum; solid line: calculated spectrum). Blue lines represent the individual doublet components. Dark blue line: $S = 0$ Fe^{II} component (6%, $\delta = 0.50$ mm·s^{-1} and $\Delta E_Q = 0.47$ mm·s^{-1}). Pale blue line: $S = 2$ Fe^{II} component (94%, $\delta = 1.12$ mm·s^{-1} and $\Delta E_Q = 2.69$ mm·s^{-1}). **c)** Mössbauer spectrum of $\mathbf{^{57}2^{IV}(O)}$ recorded in acetonitrile at 80 K in the absence of magnetic field (vertical bars: experimental spectrum; solid line: calculated spectrum using the following values of isomer shift and quadrupole splitting $\delta = 0.09$ mm·s^{-1} and $\Delta E_Q = 0.39$ mm·s^{-1}). (For interpretation of the references to colour in this figure legend, the reader is referred to the web version of this article.)

presence of a high spin and a low spin component in an approximate 1:1 ratio [36]. The Mössbauer spectrum of $\mathbf{2^{II}}$ is reported for the first time here and, in contrast, it is composed by a high spin component accounting for 94% of the sample, while the low spin species represents the residual 6% of the iron content (Fig. 3b). From all these spectroscopic data, one can conclude that the ^{Np,H}Pytacn ligand exerts a weaker crystal field than ^{Me,H}Pytacn, despite the alkylated N atoms are better σ donors in the former. According to the Mössbauer analysis, the situation is even more pronounced for ^{Me,Me}Pytacn, for which the high spin configuration is clearly more accessible. The steric demands of the neopentyl substituents in $\mathbf{1^{II}}$ prevent the tacn cycle from adopting the more compact conformation required for shortening Fe–N_{tacn} bonds. In the case of $\mathbf{2^{II}}$, the methyl group in the α position of the pyridine ring sterically interacts with the iron center, which disfavors the formation of the shorter Fe–N bonds characteristic of the low spin configuration. The impact of steric interactions in the spin state of iron(II) centers has been previously reported for Pytacn and related systems [40].

2.2. Synthesis and characterization of iron(IV)-oxo complexes

While the iron(IV)-oxo species derived from $\mathbf{1^{II}}$ and $\mathbf{3^{II}}$, [Fe^{IV}(O)(^{Np,H}Pytacn)(S)]$^{2+}$ and ($\mathbf{1^{IV}(O)}$) [Fe^{IV}(O)(^{Me,H}Pytacn)(S)]$^{2+}$ ($\mathbf{3^{IV}(O)}$), have been previously described [36,37], this is not the case for $\mathbf{2^{II}}$. Generation of its corresponding iron(IV)-oxo complex was achieved by reaction $\mathbf{2^{II}}$ with 1 equiv. of tetrabutyl ammonium periodate (Bu_4NIO_4) and 0.75 equiv. of a superacid (either bis(trifluoromethane)sulfonamide, Tf_2NH or triflic acid, TfOH) in acetonitrile at −40 °C, a methodology that is also appropriate to efficiently generate $\mathbf{1^{IV}(O)}$ and $\mathbf{3^{IV}(O)}$ (Scheme 2). Under these conditions, the iron(IV)-oxo complex [Fe^{IV}(O)(^{Me,Me}Pytacn)(S)]$^{2+}$ ($\mathbf{2^{IV}(O)}$) was immediately generated as ascertained by UV–Vis spectroscopy. The nature of the sixth ligand S in these iron(IV)-oxo compounds cannot be unambiguously established but it is likely to be an acetonitrile ligand based on literature precedents for reported iron(IV)-oxo complexes with tetradentate ligands [36,37].

Complex $\mathbf{2^{IV}(O)}$ shows an absorption spectrum with overlapping bands with λ_{max} = 797 nm (ε = 160 M^{-1} cm^{-1}), 935 nm (ε = 130 M^{-1} cm^{-1}) and 994 nm (ε = 120 M^{-1} cm^{-1}) (Fig. 3a), which is suggestive of an iron(IV)-oxo compound [41]. CSI-MS analysis of an acetonitrile solution of $\mathbf{2^{IV}(O)}$ at −40 °C further confirmed the formation of the iron(IV)-oxo compound as it exhibited the presence of a major peak at *m/z* = 483.0930 with a mass value and isotopic pattern fully consistent with [[Fe^{IV}(O)(^{Me,Me}Pytacn)](CF_3SO_3)]$^+$ (Fig. S6). Interestingly, Mössbauer spectroscopy showed only one species (>99% purity) with an isomer shift δ = 0.09 mm·s^{-1} and a quadrupole splitting ΔE_Q = 0.39 mm·s^{-1} (Fig. 3c). Experiments performed at different applied magnetic fields are in agreement with a S = 1 spin state of the iron(IV) center (Fig. S8). Similar Mössbauer parameters were previously observed for compounds $\mathbf{1^{IV}(O)}$ (δ = 0.06 mm·s^{-1}, ΔE_Q = 1.00 mm·s^{-1}) and $\mathbf{3^{IV}(O)}$ (δ = 0.05 mm·s^{-1}, ΔE_Q = 0.73 mm·s^{-1}) [36,37], which were also described as S = 1 species according to spectra recorded in applied magnetic fields. Thus, the three iron(IV)-oxo complexes studied in the present work have a S = 1 electronic structure in their ground state.

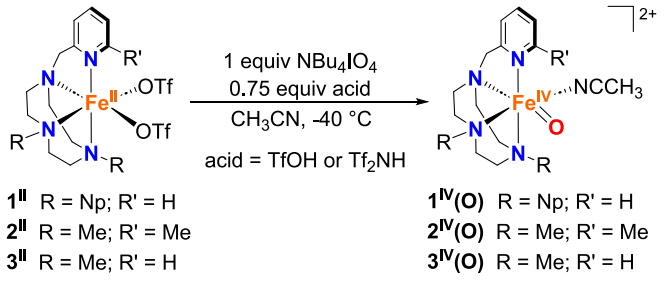

Scheme 2. Synthesis of the iron(IV)-oxo complexes used in this work from their corresponding iron(II) precursors. Compounds $\mathbf{1^{IV}(O)}$ and $\mathbf{3^{IV}(O)}$ have been previously reported [36,37] while synthesis and characterization of $\mathbf{2^{IV}(O)}$ is described here for the first time.

2.3. Chlorination reactions

Initial tests for the reactivity studies were carried out with compound $\mathbf{1^{IV}(O)}$. In the presence of 10 equiv. NBu_4Cl, the reaction of $\mathbf{1^{IV}(O)}$ with ethylbenzene (550 equiv) under N_2 was monitored by UV–Vis spectroscopy and organic products were analyzed when its characteristic absorption band at 760 nm had completely disappeared. GC analysis at the end of the reaction showed that only oxygenated products were formed under these conditions: 0.19 equiv. of acetophenone and 0.14 equiv. of 1-phenethyl alcohol with respect to $\mathbf{1^{IV}(O)}$ (entry 1, Fig. 4). Considering that the decay of $\mathbf{1^{IV}(O)}$ produces exclusively Fe^{III} species as ascertained by MS analysis (Fig. S16), we conclude that each molecule of $\mathbf{1^{IV}(O)}$ formally behaves as a single electron oxidant. Therefore, detected organic oxidation products in this experiment account for ~99% of the oxidizing equivalents.

Most remarkably, introduction of protons by using the superacid Tf_2NH within the reaction mixture provoked a drastic change in product selectivity, favoring the generation of organic halogenated instead of oxygenated products. Reaction of $\mathbf{1^{IV}(O)}$ with ethylbenzene (550 equiv) in a solution containing NBu_4Cl (10 equiv), Tf_2NH (32 equiv), and acetic acid (200 equiv) under N_2 was also monitored by UV–Vis spectroscopy (Fig. S11). The reaction mixture was again analyzed when the 760 nm absorption band characteristic of $\mathbf{1^{IV}(O)}$ had completely disappeared. GC and GC–MS analyses of the organic products in the final reaction mixtures indicated the generation of (1-chloroethyl)benzene as main product (0.41 equiv. with respect to $\mathbf{1^{IV}(O)}$), together with a smaller amount of acetophenone (0.08 equiv), 1-phenylethanol (0.06 equiv) and *ortho/para*-chloroethylbenzene (0.03 equiv) (entry 2, Fig. 4). Exclusive chlorination and improved yields for the production of (1-chloroethyl) benzene (0.45 equiv. with respect to $\mathbf{1^{IV}(O)}$), were observed when deuterated acetonitrile was employed (entry 3, Fig. 4). This accounts for a 90% yield of ethylbenzene chlorination in this reaction.

Blank experiments in the absence of superacid or iron showed no formation of chlorination products (entries 4 and 9, Fig. 4). Moreover, a control experiment combining phenylethanol, the superacid and the chloride under the standard reaction conditions (with and without $\mathbf{1^{IV}(O)}$) afforded no chlorinated product. Thus, it can be discarded that the chlorination product is formed from 1-phenylethanol.

Ethylbenzene chlorination was also observed when the reaction was conducted in the absence of acetic acid, albeit in lower yields and reduced selectivity (entry 5, Fig. 4). Acetophenone and 1-phenylethanol were obtained as major products (0.10 equiv. of acetophenone and 0.13 equiv. of 1-phenylethanol) together with small quantities of (1-chloroethyl)benzene (0.03 equiv). The distribution of products was drastically affected when reactions were performed under O_2 or air atmosphere instead of N_2 (entry 6 and 7, Fig. 4). When the reaction was run in the presence of O_2, the amount of acetophenone increased up to ~0.25 equiv. with residual amounts of alcohol or chlorinated products, suggesting that O_2 is incorporated into products via trapping of long-lived benzyl radicals.

Bromination of ethylbenzene was achieved in an efficient manner under the same reaction conditions, employing NBu_4Br (1.5 equiv) instead of NBu_4Cl (entry 8, Fig. 4) obtaining (1-bromoethyl)benzene as the major product (0.35 equiv. with respect to $\mathbf{1^{IV}(O)}$) together with acetophenone (0.12 equiv) and traces of 1-phenylethanol. Higher bromide loadings caused rapid decay of $\mathbf{1^{IV}(O)}$ and reduced product yields, probably due to oxidation of Br^- to produce bromine radicals.

In conclusion, addition of protons diverts the chemoselectivity of $\mathbf{1^{IV}(O)}$ in C–H functionalization, which changes from exclusive oxygenation towards performing selective and nearly quantitative chlorination and bromination of aliphatic C–H bonds.

Other substrates different from ethylbenzene also underwent functionalization. When cumene was used as substrate, α-dimethyl benzyl

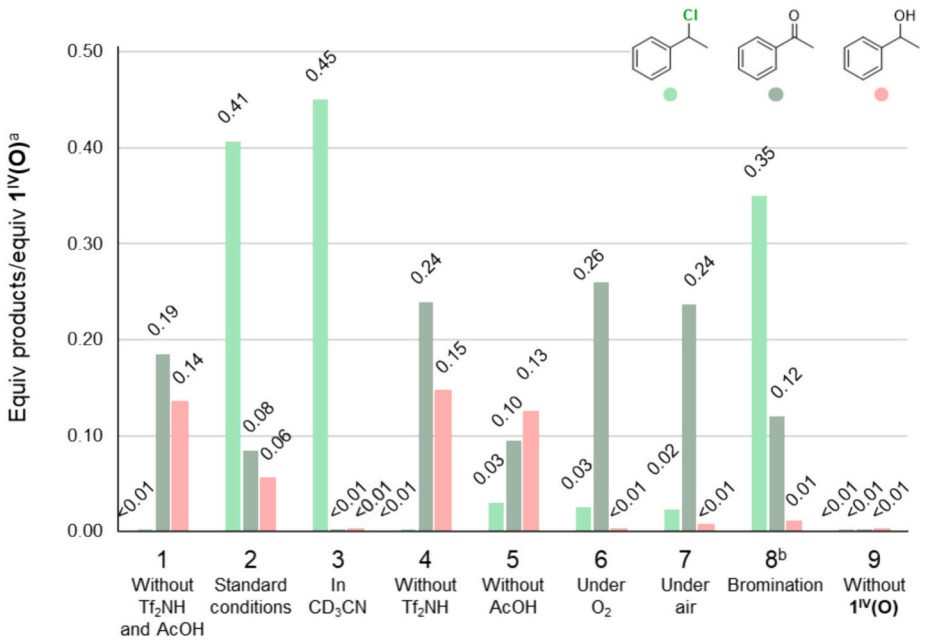

Fig. 4. Amounts of products obtained in the reaction of $\mathbf{1^{IV}(O)}$ (1 mM) with ethylbenzene (0.5 M) in CH_3CN at −40 °C. Variation from the standard reaction conditions (10 equiv. NBu_4Cl, 32 equiv. Tf_2NH and 200 equiv. AcOH at −40 °C under a N_2 atmosphere) are indicated below each entry. [a]Equivalents of product are calculated versus the initial amount of Fe^{II} employed to generate $\mathbf{1^{IV}(O)}$ (2 μmols). [b]1.5 equiv. NBu_4Br were used instead of 10 equiv. NBu_4Cl.

chloride (0.32 equiv. with respect to $\mathbf{1^{IV}(O)}$) was obtained together with large amounts of α-dimethyl benzyl alcohol (0.54 equiv) (entry 5, Fig. 5), thus affording somehow low chlorination selectivity. Remarkably, stronger C–H bonds such as the benzylic protons of toluene (BDE = 89.7 kcal·mol^{-1}) were also functionalized. Benzyl chloride was obtained as the main product (0.15 equiv. with respect to $\mathbf{1^{IV}(O)}$) together with smaller amounts of the oxygenated products (0.09 equiv) (entry 6, Fig. 5). When the halogenation reaction was carried out using substrates containing even stronger C–H bonds such as 2,3-dimethylbutane, cyclooctane and cyclohexane only very poor yields and selectivities were obtained. For 2,3-dimethylbutane, 2-chloro-2,3-dimethylbutane and 2,3-dimethyl-2-butanol were obtained in similar amounts accounting for 0.02 equiv. each (entry 7, Fig. 5). When the reaction was carried out using cyclohexane or cyclooctane as substrates, chlorinated products and ketones were obtained as 1:1 mixtures, representing between 0.01 and 0.02 equiv. of products with respect to $\mathbf{1^{IV}(O)}$ (entries 9 and 11, Fig. 5).

The other structurally-related iron(IV)-oxo complexes proposed in this work were also tested as chemoselective chlorinating agents under the above mentioned conditions. Interestingly, compound $\mathbf{2^{IV}(O)}$ and $\mathbf{3^{IV}(O)}$ could efficiently chlorinate ethylbenzene, affording 0.38 equiv. and 0.14 equiv. of (1-chloroethyl)benzene, respectively (entries 2 and 3, Fig. 5). While a good selectivity for the chlorinated product was observed for $\mathbf{2^{IV}(O)}$, $\mathbf{3^{IV}(O)}$ afforded significant amounts of acetophenone. Noteworthy and analogously to $\mathbf{1^{IV}(O)}$, no traces of chlorinated product were observed in blank experiments in the absence of acid. Given the promising results with $\mathbf{2^{IV}(O)}$, the oxidation of substrates with stronger C–H bonds was also attempted with this compound. Reaction of $\mathbf{2^{IV}(O)}$ with 2,3-dimethylbutane produced 0.15 equiv. 2-chloro-2,3-dimethylbutane along with 0.04 equiv. of the corresponding alcohol

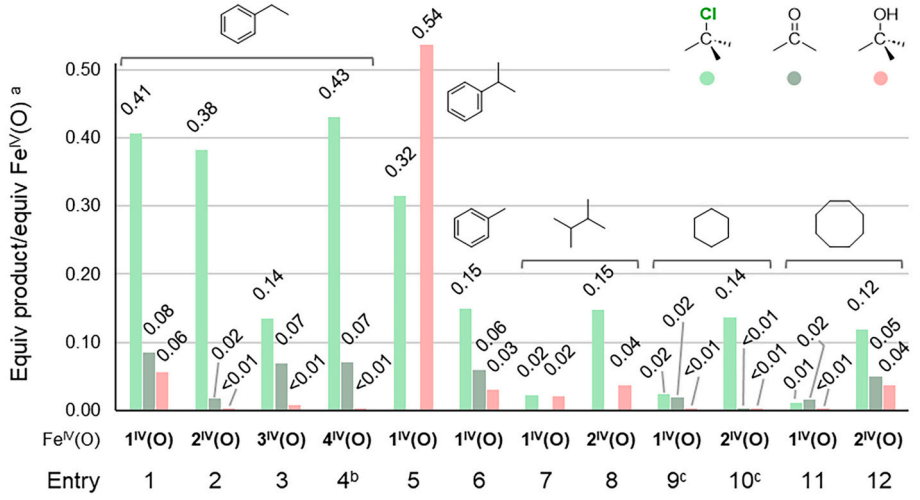

Fig. 5. Amounts of products obtained for the reactions of $\mathbf{1^{IV}(O)}$, $\mathbf{2^{IV}(O)}$, $\mathbf{3^{IV}(O)}$ and $\mathbf{4^{IV}(O)}$ (1 mM) with a set of substrates in the presence of 10 equiv. NBu_4Cl, 32 equiv. Tf_2NH and 200 equiv. AcOH in CH_3CN at −40 °C under a N_2 atmosphere. [a] Calculated versus the initial amount of Fe^{II} employed to generate $\mathbf{1^{IV}(O)}$, $\mathbf{2^{IV}(O)}$, $\mathbf{3^{IV}(O)}$ and $\mathbf{4^{IV}(O)}$ (2 μmols). [b] Reaction performed at +20 °C. [c] Reaction performed at −20 °C.

(entry 8, Fig. 5), which accounts for a 38% overall yield and 79% selectivity for the chlorinated product. These numbers contrast with the much more modest results obtained with $\mathbf{1^{IV}(O)}$ exhibiting only 8% yield and no preference for the chlorination over the oxygenation. Reaction of cyclooctane with $\mathbf{2^{IV}(O)}$ afforded 0.12 equiv. of chlorocyclooctane (entry 12, Fig. 5), in contrast with the 0.01 equiv. obtained with $\mathbf{1^{IV}(O)}$ under the same conditions. Remarkably, the selectivity for the chlorination product with $\mathbf{2^{IV}(O)}$ was rather modest as significant amounts of oxidized products (0.05 equiv. cyclooctanone and 0.04 equiv. cyclooctanol) were also detected. Finally, reaction with cyclohexane showed a dramatic improvement both in yields and selectivity when using compound $\mathbf{2^{IV}(O)}$ instead of $\mathbf{1^{IV}(O)}$. For this particular substrate, reactions were extremely slow at −40 °C so that they were carried out at −20 °C, instead. Remarkably, exclusive formation of 0.14 equiv. of chlorocyclohexane were detected using $\mathbf{2^{IV}(O)}$ accounting for 28% yield. In contrast, only 0.02 equiv. of chlorocyclohexane (4% yield) were obtained with $\mathbf{1^{IV}(O)}$ along with similar amounts of cyclohexanone.

We currently do not fully understand the reason why $\mathbf{2^{IV}(O)}$ is the best compound from the series in the chlorination of strong C–H bonds. However, according to the characterization of the corresponding iron(II) complexes ($\mathbf{1^{II}}$, $\mathbf{2^{II}}$ and $\mathbf{3^{II}}$, see above) the substituents in the Pytacn ligand have a significant impact on the accessibility of the high spin state. Thus, the ^{Me,Me}Pytacn in $\mathbf{2^{II}}$ is a weaker field ligand than ^{Np,H}Pytacn in $\mathbf{1^{II}}$, making the high spin state more favorable for the former as clearly evidenced from the Mössbauer analysis (see above). Considering that previous studies showed that the reactivity of iron(IV)-oxo species occurs through the S = 2 energy surface [42–44], one may hypothesize that the higher accessibility of the high spin state imposed by the ^{Me,Me}Pytacn in $\mathbf{2^{IV}(O)}$ makes this compound more reactive and thus, more efficient in the activation and chlorination of stronger C–H bonds. In sharp contrast, the ^{Me,H}Pytacn ligand, which behaves as a stronger field ligand affording the low spin iron(II) precursor $\mathbf{3^{II}}$, gives rise to $\mathbf{3^{IV}(O)}$ with remarkably poorer activities than $\mathbf{1^{IV}(O)}$ and $\mathbf{2^{IV}(O)}$.

2.4. Insight into the reactive species

Spectroscopic and mass spectrometry analysis of $\mathbf{1^{IV}(O)}$ under reaction conditions strongly suggests that the halide does not bind to the metal center. In first place, addition of tetrabutyl ammonium chloride (NBu_4Cl, 10 equiv) or HCl (10 equiv) to $\mathbf{1^{IV}(O)}$ did not cause changes in its UV–Vis spectrum. Thus, the characteristic band shifts previously described for the binding of chloride anions at iron(IV)-oxo species [28,30] in *cis*-position to the oxo-ligand were not observed, attesting that chloride does not bind to $\mathbf{1^{IV}(O)}$. In addition, CSI-MS analyses performed after HCl addition, denoted the presence of cluster peaks at $m/z = 581.2038$ with an isotopic pattern fully consistent a $[[Fe^{IV}(O)(^{Np,H}Pytacn)](CF_3SO_3)]^+$ formulation (Fig. S19); the same signal was observed in the absence of a chloride anion source (NBu_4Cl or HCl). Barely a minor signal, consistent with $[Fe^{IV}(O)(L)(Cl)]^+$, is observed in the case of HCl (10 equiv) addition to $\mathbf{1^{IV}(O)}$. Thus, both UV–Vis and CSI-MS analyses suggest that the chloride anions do not occupy the sixth *cis*-labile coordinative position under the present conditions.

In order to gain further support that chloride binding is not a requisite for chemoselective chlorination, the iron(IV)-oxo complex $[Fe(O)(N4Py)]^{2+}$ ($\mathbf{4^{IV}(O)}$) based on the pentadentate ligand N4Py [45–47] was also tested for the oxidative chlorination of ethylbenzene under the same acidic reaction conditions. $\mathbf{4^{IV}(O)}$ did not react with ethylbenzene at −40 °C. However, when performing the reaction at +20 °C, 0.43 equiv. of (1-chloroethyl)benzene with respect to $\mathbf{4^{IV}(O)}$ were produced as main product (entry 4, Fig. 5). Overall, these experiments confirm that chloride binding is not necessary for the production of chlorinated products.

2.5. Kinetic analysis of the reactions

Insight into the reaction mechanism was derived from kinetic analyses. Monitoring of the reaction between $\mathbf{1^{IV}(O)}$ and different substrates under standard chlorination conditions was done by following the decay of its low energy absorption band at 760 nm. Decays followed a first order exponential behavior (Fig. S11) and rate constants linearly increased by increasing substrate concentration (Fig. S12), indicating that these are bimolecular processes. From the slope of these linear correlations, second order rate constants (k_2) could be extracted. Apart from ethylbenzene, alkanes with different C–H bond dissociation energies (BDE) were used, including dihydroanthracene (DHA), fluorene, triphenylmethane (Ph_3CH) and cumene. k_2 values for each substrate were adjusted to account for the number of equivalent C–H bonds contained in the substrate (k_2') and they were found to decrease with the increase in the strength of the C–H bond (BDE). Furthermore, log(k_2') correlated linearly with BDE values (**Fig. 6**). This linear correlation is consistent with a hydrogen atom transfer (HAT) being the rate-determining step for the consumption of $\mathbf{1^{IV}(O)}$ [18,30,32,33]. Additionally, a kinetic isotope effect (KIE) of 45 was observed when the reaction was performed with deuterated DHA (DHA-d_4) (Fig. S15). This large KIE value overpasses the semi-classical limit of 7, suggesting that the HAT mechanism is dominated by quantum mechanical tunneling [48–50], as was previously found for other iron(IV)-oxo systems [37,51,52]. Moreover, such large KIEs have also been observed in HAT reactions performed by the iron(IV)-oxo intermediate of TauD (KIE = 37) [53].

Analogous kinetic analyses were also performed when the same reactions were conducted in the absence of the halide source (NBu_4Cl) and also in the absence of both the acids and halide source. The plots showing the dependence of log(k_2') versus substrate C–H BDE were almost superimposable with that obtained for the standard chlorination conditions (Fig. S14). Moreover, KIEs were also of the same magnitude under the three different reaction conditions (Fig. S15). Thus, a KIE value of 49 was determined in the absence of the halide source, while this number was 41 in the absence of both acids and halide source. Altogether, this data indicates that the HAT step is not sensitive to the presence of acid or halide providing compelling evidence that the HAT is performed by the same species, irrespective of the presence or absence of the halide source or the acid.

Overall, we propose that the halogenation is initiated through a HAT accomplished by $\mathbf{1^{IV}(O)}$, generating Fe^{III} species and a long-lived carbon-centered radical (Scheme 3). This initial step represents the rate-determining step (rds) of the process, as settled by the second order rate constants linearity versus the C–H BDE of different substrates and large kinetic isotope effects. Changes in the chemoselectivity of the reaction upon acid addition must then originate after HAT. We hypothesize that under acidic conditions the iron(III)-hydroxo species formed after the HAT is protonated to form an iron(III)-aqua species (Scheme 3). This is followed by an exchange of the coordinated aquo ligand by a chloride forming an iron(III)-chloride species. The homolytic cleavage of the Fe^{III}-Cl species provides a chlorine radical which reacts with the carbon-centered radical, producing the corresponding halogenated product. Alternatively, the C–Cl bond may result from bimolecular reaction of the carbon-centered radical with the Fe^{III}–Cl bond. The resulting iron(II) undergoes fast oxidation with a second molecule of unreacted iron(IV)-oxo, resulting in the finally detected ferric complexes. The latter comproportionation reaction explains the roughly maximum 0.5 equiv. of halogenated products with respect to Fe observed. This mechanism is supported by the fact that the carbon-centered radical generated under acidic conditions must be long lived as it can be quenched by O_2 and that halide binding to the iron(IV)-oxo is not a requisite for halogenation.

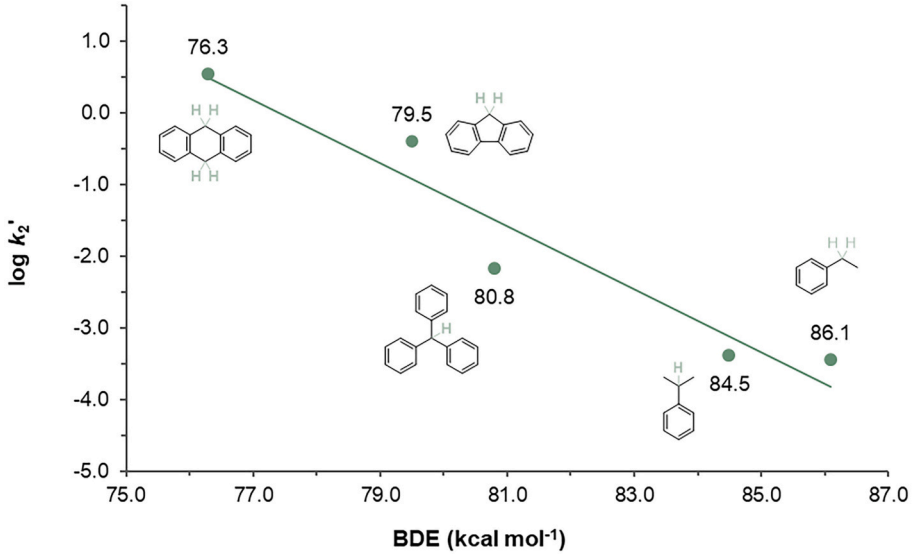

Fig. 6. Plot of log(k_2') against the C–H BDE of different substrates for the reaction of $\mathbf{1^{IV}(O)}$ under standard chlorination conditions (presence of 10 equiv. NBu_4Cl, 32 equiv. Tf_2NH and 200 equiv. AcOH in CH_3CN at −40 °C under a N_2 atmosphere).

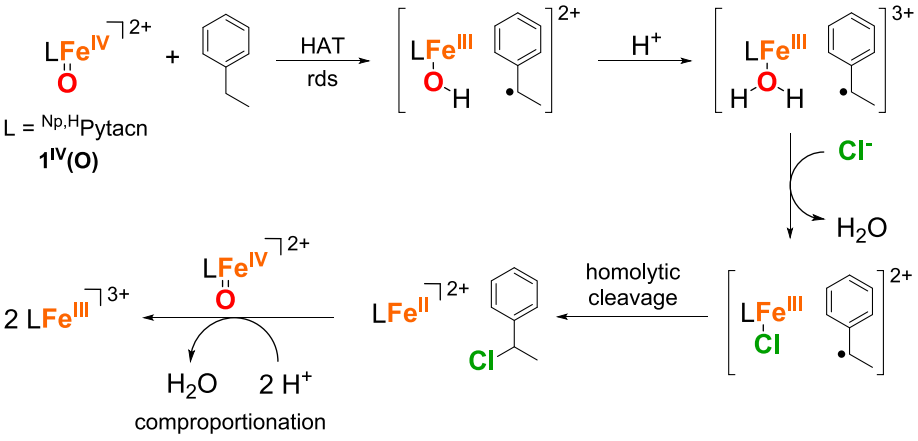

Scheme 3. Proposed mechanism of the reaction of $\mathbf{1^{IV}(O)}$ with ethylbenzene.

Conclusions

In this work we have disclosed the ability of iron(IV)-oxo species $\mathbf{1^{IV}(O)}$, $\mathbf{2^{IV}(O)}$ and $\mathbf{3^{IV}(O)}$ to halogenate hydrocarbons when the reactions are performed in the presence of a strong acid. The efficiency and selectivity for the halogenated products is particularly remarkable for $\mathbf{1^{IV}(O)}$ and $\mathbf{2^{IV}(O)}$, whose ligand architectures are more sterically hindered making the high spin state of the iron center more accessible. Almost quantitative yields for the chlorination of ethylbenzene are detected for both compounds with only residual amounts of oxygenated products. The reaction can be extended to other substrates bearing benzylic C–H bonds and even stronger aliphatic C–H bonds. Particularly remarkable is the chlorination of cyclohexane and cyclooctane with modest yields but relatively high selectivities by compound $\mathbf{2^{IV}(O)}$, which contrasts with the poor results obtained by $\mathbf{1^{IV}(O)}$. In order to explain these results, two considerations related to accessibility and reactivity of the different spin states should be taken into account: firstly, the characterization of the iron(II) precursors indicates that ligand ^{Me,Me}Pytacn is a weaker field ligand than ^{Np,H}Pytacn and secondly, previous studies suggest that the reactivity of iron(IV)-oxo species is higher in the S = 2 energy surface rather than in S = 1. Thus, the markedly more efficient chlorination of strong alkyl C–H bonds by $\mathbf{2^{IV}(O)}$ compared to $\mathbf{1^{IV}(O)}$, strongly supports the idea that the higher accessibility of the high-spin state in the former is beneficial for the halogenation of these bonds.

According to our kinetic studies, a chlorination mechanism entailing a HAT by the iron(IV)-oxo species affording a free-diffusing carbon-centered radical and an iron(III)-hydroxo species is proposed. This step is not affected by the presence of acid so that the chemoselectivity is dictated afterwards. We propose that under acidic conditions the iron (III)-hydroxo species gets protonated to form an iron(III)-aqua complex, and subsequently a chloride anion substitutes the aqua ligand. Reaction of the alkyl radical with the Fe^{III}–Cl bond affords the observed chlorinated products. Thus, from our analyses we conclude that HAT is very likely executed by the same species and final chlorination or hydroxylation depends on the subsequent step. Our data shows no evidence for binding of the chloride at the iron(IV)-oxo center, but instead we speculate that binding, and replacement of a water molecule occurs after hydrogen abstraction. Overall, the present report represents the first example of a halogenase functional model in which protonation seems to be required to achieve exquisite selectivity for C–H bond halogenation.

CRediT authorship contribution statement

Neus Pagès-Vilà: Writing – review & editing, Methodology,

Investigation. **Ilaria Gamba:** Writing – original draft, Methodology, Investigation, Formal analysis. **Martin Clémancey:** Investigation. **Jean-Marc Latour:** Investigation. **Anna Company:** Writing – review & editing, Supervision, Funding acquisition. **Miquel Costas:** Writing – review & editing, Writing – original draft, Resources, Investigation.

Declaration of competing interest

The authors declare that they have no known competing financial interests or personal relationships that could have appeared to influence the work reported in this paper.

Data availability

Data will be made available on request.

Acknowledgements

The authors thank the Spanish Ministry of Science (PID2019-106699GB-I00 to A.C. and PID2021-129036NB-I00 to M.C.) and Generalitat de Catalunya (ICREA Academia Award and 2021SGR00475 project to M.C. and A.C.) for financial support. M.C. thanks financial support from the European Research Council (ERC-2019-ADG-883922). Open Access funding provided thanks to the CRUE-CSIC agreement with Elsevier.

Appendix A. Supplementary data

Supplementary data to this article can be found online at https://doi.org/10.1016/j.jinorgbio.2024.112643.

References

[1] V. Agarwal, Z.D. Miles, J.M. Winter, A.S. Eustáquio, A.A. El Gamal, B.S. Moore, Enzymatic halogenation and dehalogenation reactions: pervasive and mechanistically diverse, Chem. Rev. 117 (2017) 5619–5674.
[2] F.H. Vaillancourt, E. Yeh, D.A. Vosburg, S. Garneau-Tsodikova, C.T. Walsh, Nature's inventory of halogenation catalysts: oxidative strategies predominate, Chem. Rev. 106 (2006) 3364–3378.
[3] L.C. Blasiak, F.H. Vaillancourt, C.T. Walsh, C.L. Drennan, Crystal structure of the non-haem iron halogenase SyrB2 in syringomycin biosynthesis, Nature 440 (2006) 368–371.
[4] S.D. Wong, M. Srnec, M.L. Matthews, L.V. Liu, Y. Kwak, K. Park, C.B. Bell Iii, E. E. Alp, J. Zhao, Y. Yoda, S. Kitao, M. Seto, C. Krebs, J.M. Bollinger, E.I. Solomon, Elucidation of the Fe(IV)=O intermediate in the catalytic cycle of the halogenase SyrB2, Nature 499 (2013) 320–323.
[5] D.P. Galonić, E.W. Barr, C.T. Walsh, J.M. Bollinger, C. Krebs, Two interconverting Fe(IV) intermediates in aliphatic chlorination by the halogenase CytC3, Nat. Chem. Biol. 3 (2007) 113–116.
[6] Martinie, R. J.; Livada, J.; Chang, W.-c.; Green, M. T.; Krebs, C.; Bollinger, J. M., Jr.; Silakov, A., Experimental correlation of substrate position with reaction outcome in the aliphatic Halogenase, SyrB2. J. Am. Chem. Soc. 2015, 137, 6912–6919.
[7] M.L. Matthews, C.S. Neumann, L.A. Miles, T.L. Grove, S.J. Booker, C. Krebs, C. T. Walsh, J.M. Bollinger, Substrate positioning controls the partition between halogenation and hydroxylation in the aliphatic halogenase, SyrB2, Proc. Natl. Acad. Sci. 106 (2009) 17723–17728.
[8] A.J. Mitchell, Q. Zhu, A.O. Maggiolo, N.R. Ananth, M.L. Hillwig, X. Liu, A.K. Boal, Structural basis for halogenation by iron- and 2-oxo-glutarate-dependent enzyme WelO5, Nat. Chem. Biol. 12 (2016) 636–640.
[9] M. Srnec, E.I. Solomon, Frontier molecular orbital contributions to chlorination versus hydroxylation selectivity in the non-Heme Iron Halogenase SyrB2, J. Am. Chem. Soc. 139 (2017) 2396–2407.
[10] J. Huang, C. Li, B. Wang, D.A. Sharon, W. Wu, S. Shaik, Selective chlorination of substrates by the Halogenase SyrB2 is controlled by the protein according to a combined quantum mechanics/molecular mechanics and molecular dynamics study, ACS Catal. 6 (2016) 2694–2704.
[11] T. Borowski, H. Noack, M. Radoń, K. Zych, P.E.M. Siegbahn, Mechanism of selective halogenation by SyrB2: a computational study, J. Am. Chem. Soc. 132 (2010) 12887–12898.
[12] H. Noack, P.E.M. Siegbahn, Theoretical investigation on the oxidative chlorination performed by a biomimetic non-heme iron catalyst, J. Biol. Inorg. Chem. 12 (2007) 1151–1162.
[13] M.G. Quesne, S.P. de Visser, Regioselectivity of substrate hydroxylation versus halogenation by a nonheme iron(IV)–oxo complex: possibility of rearrangement pathways, J. Biol. Inorg. Chem. 17 (2012) 841–852.
[14] R. Mehmood, V. Vennelakanti, H.J. Kulik, Spectroscopically guided simulations reveal distinct strategies for positioning substrates to achieve selectivity in Nonheme Fe(II)/α-ketoglutarate-dependent Halogenases, ACS Catal. 11 (2021) 12394–12408.
[15] R. Mehmood, H.W. Qi, A.H. Steeves, H.J. Kulik, The Protein's role in substrate positioning and reactivity for biosynthetic enzyme complexes: the case of SyrB2/SyrB1, ACS Catal. 9 (2019) 4930–4943.
[16] M.L. Matthews, C.S. Neumann, L.A. Miles, T.L. Grove, S.J. Booker, C. Krebs, C. T. Walsh, J.M. Bollinger, Substrate positioning controls the partition between halogenation and hydroxylation in the aliphatic halogenase, SyrB2, Proc. Natl. Acad. Sci. USA 106 (2009) 17723–17728.
[17] R. Breslow, Biomimetic chemistry: biology as an inspiration, J. Biol. Chem. 284 (2009) 1337–1342.
[18] R.H. Holm, E.I. Solomon, Preface: biomimetic inorganic chemistry, Chem. Rev. 104 (2004) 347–348.
[19] V. Yadav, R.J. Rodriguez, M.A. Siegler, D.P. Goldberg, Determining the inherent selectivity for carbon radical hydroxylation versus halogenation with $Fe^{III}(OH)(X)$ complexes: relevance to the rebound step in non-heme Iron Halogenases, J. Am. Chem. Soc. 142 (2020) 7259–7264.
[20] E.F. Gérard, V. Yadav, D.P. Goldberg, S.P. de Visser, What drives radical halogenation versus hydroxylation in mononuclear Nonheme Iron complexes? A combined experimental and computational study, J. Am. Chem. Soc. 144 (2022) 10752–10767.
[21] R.A. Leising, Y. Zang, L. Que Jr., Oxidative ligand transfer to alkanes: a model for iron-mediated C-X bond formation in beta-lactam antibiotic biosynthesis, J. Am. Chem. Soc. 113 (1991) 8555–8557.
[22] T. Kojima, R.A. Leising, S. Yan, L. Que Jr., Alkane functionalization at nonheme iron centers. Stoichiometric transfer of metal-bound ligands to alkane, J. Am. Chem. Soc. 115 (1993) 11328–11335.
[23] S. Chatterjee, T.K. Paine, Hydroxylation versus Halogenation of Aliphatic C–H Bonds by a Dioxygen-Derived Iron–Oxygen Oxidant: Functional Mimicking of Iron Halogenases, Angew. Chem. Int. Ed. 55 (2016) 7717–7722.
[24] R.D. Jana, D. Sheet, S. Chatterjee, T.K. Paine, Aliphatic C–H Bond Halogenation by Iron(II)-α-Keto Acid Complexes and O_2: Functional Mimicking of Nonheme Iron Halogenases, Inorg. Chem. 57 (2018) 8769–8777.
[25] K. Bleher, P. Comba, D. Faltermeier, A. Gupta, M. Kerscher, S. Krieg, B. Martin, G. Velmurugan, S. Yang, Non-Heme-Iron-mediated selective halogenation of Unactivated carbon−hydrogen bonds, Chem. Eur. J. 28 (2022) e202103452.
[26] P. Comba, S. Wunderlich, Iron-catalyzed halogenation of alkanes: modeling of Nonheme Halogenases by experiment and DFT calculations, Chem. Eur. J. 16 (2010) 7293–7299.
[27] C. Shen, W.M. Dagnaw, C.W. Fong, K.C. Lau, C.-F. Chow, Selective functionalization of C(sp3)–H bonds: catalytic chlorination and bromination by IronIII-acacen-halide under ambient condition, Chem. Commun. 58 (2022) 10627–10630.
[28] J.-U. Rohde, A. Stubna, E.L. Bominaar, E. Münck, W. Nam, L. Que, Nonheme Oxoiron(IV) complexes of Tris(2-pyridylmethyl)amine with *cis*-Monoanionic ligands, Inorg. Chem. 45 (2006) 6435–6445.
[29] J. England, Y. Guo, K.M. Van Heuvelen, M.A. Cranswick, G.T. Rohde, E. L. Bominaar, E. Münck, L. Que Jr., A more reactive trigonal-Bipyramidal high-spin Oxoiron(IV) complex with a cis-labile site, J. Am. Chem. Soc. 133 (2011) 11880–11883.
[30] O. Planas, M. Clémancey, J.-M. Latour, A. Company, M. Costas, Structural modeling of iron halogenases: synthesis and reactivity of halide-iron(IV)-oxo compounds, Chem. Commun. 50 (2014) 10887–10890.
[31] M. Puri, A.N. Biswas, R. Fan, Y. Guo, L. Que Jr., Modeling Non-Heme Iron Halogenases: High-Spin Oxoiron(IV)–Halide Complexes That Halogenate C–H Bonds, J. Am. Chem. Soc. 138 (2016) 2484–2487.
[32] T. Terencio, E. Andris, I. Gamba, M. Srnec, M. Costas, J. Roithová, Chemoselectivity in the oxidation of Cycloalkenes with a non-Heme Iron(IV)-Oxo-chloride complex: epoxidation vs. hydroxylation selectivity, J. Am. Soc. Mass Spectrom. 30 (2019) 1923–1933.
[33] S. Rana, J.P. Biswas, A. Sen, M. Clémancey, G. Blondin, J.-M. Latour, G. Rajaraman, D. Maiti, Selective C–H halogenation over hydroxylation by non-heme iron(IV)-oxo, Chem. Sci. 9 (2018) 7843–7858.
[34] A. Company, L. Gómez, X. Fontrodona, X. Ribas, M. Costas, A novel platform for modeling oxidative catalysis in non-Heme Iron Oxygenases with unprecedented efficiency, Chem. Eur. J. 14 (2008) 5727–5731.
[35] A. Company, L. Gómez, M. Güell, X. Ribas, J.M. Luis, L. Que, M. Costas, Alkane hydroxylation by a Nonheme Iron catalyst that challenges the Heme paradigm for oxygenase action, J. Am. Chem. Soc. 129 (2007) 15766–15767.
[36] C.E. Castillo, I. Gamba, L. Vicens, M. Clémancey, J.-M. Latour, M. Costas, M. G. Basallote, Spin state Tunes oxygen atom transfer towards $Fe^{IV}O$ formation in Fe^{II} complexes, Chem. Eur. J. 27 (2021) 4946–4954.
[37] A. Company, I. Prat, J.R. Frisch, D.R. Mas-Ballesté, M. Güell, G. Juhász, X. Ribas, D. E. Münck, J.M. Luis, L. Que, M. Costas, Modeling the *cis*-Oxo-labile binding site motif of non-Heme Iron Oxygenases: water exchange and oxidation reactivity of a non-Heme Iron(IV)-Oxo compound bearing a Tripodal Tetradentate ligand, Chem. Eur. J. 17 (2011) 1622–1634.
[38] I. Prat, L. Gómez, M. Canta, X. Ribas, M. Costas, An Iron catalyst for oxidation of alkyl C-H bonds showing enhanced selectivity for Methylenic sites, Chem. Eur. J. 19 (2013) 1908–1913.
[39] Compound $\mathbf{2^{II}}$ with coordinated triflate anions crystallizes out as very thin needles, which are not suitable for X-ray diffraction. Only the spontaneously formed crystals of the iron(II) bis-aquo complex (from adventitious water) can be analyzed by X-ray diffraction.

[40] I. Prat, A. Company, T. Corona, T. Parella, X. Ribas, M. Costas, Assessing the impact of electronic and steric tuning of the ligand in the spin state and catalytic oxidation ability of the Fe^{II}(Pytacn) family of complexes, Inorg. Chem. 52 (2013) 9229–9244.
[41] A.R. McDonald, L. Que, High-valent nonheme iron-oxo complexes: synthesis, structure, and spectroscopy, Coord. Chem. Rev. 257 (2013) 414–428.
[42] M.S. Seo, N.H. Kim, K.-B. Cho, J.E. So, S.K. Park, M. Clémancey, R. Garcia-Serres, J.-M. Latour, S. Shaik, W. Nam, A mononuclear nonheme iron(IV)-oxo complex which is more reactive than cytochrome P450 model compound I, Chem. Sci. 2 (2011) 1039–1045.
[43] H. Hirao, D. Kumar, L. Que Jr., S. Shaik, Two-state reactivity in alkane hydroxylation by non-Heme Iron−Oxo complexes, J. Am. Chem. Soc. 128 (2006) 8590–8606.
[44] D. Janardanan, Y. Wang, P. Schyman, L. Que Jr., S. Shaik, The fundamental role of exchange-enhanced reactivity in C-H activation by S=2 Oxo Iron(IV) complexes, Angew. Chem. Int. Ed. 49 (2010) 3342–3345.
[45] G. Roelfes, M. Lubben, K. Chen, R.Y.N. Ho, A. Meetsma, S. Genseberger, R. M. Hermant, R. Hage, S.K. Mandal, V.G. Young, Y. Zang, H. Kooijman, A.L. Spek, L. Que, B.L. Feringa, Iron chemistry of a Pentadentate ligand that generates a metastable Fe^{III}−OOH intermediate, Inorg. Chem. 38 (1999) 1929–1936.
[46] J. Kaizer, E.J. Klinker, N.Y. Oh, J.-U. Rohde, W.J. Song, A. Stubna, J. Kim, E. Münck, W. Nam, L. Que, Nonheme Fe^{IV}O complexes that can oxidize the C−H bonds of cyclohexane at room temperature, J. Am. Chem. Soc. 126 (2004) 472–473.
[47] E.J. Klinker, J. Kaizer, W.W. Brennessel, N.L. Woodrum, C.J. Cramer, L. Que Jr., Structures of Nonheme Oxoiron(IV) complexes from X-ray crystallography, NMR spectroscopy, and DFT calculations, Angew. Chem. Int. Ed. 44 (2005) 3690–3694.
[48] A. Kohen, J.P. Klinman, Enzyme catalysis: beyond classical paradigms, Acc. Chem. Res. 31 (1998) 397–404.
[49] Z. Pan, J.H. Horner, M. Newcomb, Tunneling in C−H oxidation reactions by an Oxoiron(IV) porphyrin radical cation: direct measurements of very large H/D kinetic isotope effects, J. Am. Chem. Soc. 130 (2008) 7776–7777.
[50] E.J. Klinker, S. Shaik, H. Hirao, L. Que, A two-state reactivity model explains unusual kinetic isotope effect patterns in C-H bond cleavage by Nonheme Oxoiron (IV) complexes, Angew. Chem. Int. Ed. 121 (2009) 1317–1321.
[51] N.Y. Oh, Y. Suh, M.J. Park, M.S. Seo, J. Kim, W. Nam, Mechanistic Insight into Alcohol Oxidation by High-Valent Iron–Oxo Complexes of Heme and Nonheme Ligands, Angew. Chem. Int. Ed. 117 (2005) 4307–4311.
[52] C.V. Sastri, J. Lee, K. Oh, Y.J. Lee, J. Lee, T.A. Jackson, K. Ray, H. Hirao, W. Shin, J. A. Halfen, J. Kim, L. Que, S. Shaik, W. Nam, Axial ligand tuning of a nonheme iron (IV)–oxo unit for hydrogen atom abstraction, Proc. Natl. Acad. Sci. USA 104 (2007) 19181–19186.
[53] J.C. Price, E.W. Barr, T.E. Glass, C. Krebs, J.M. Bollinger, Evidence for hydrogen abstraction from C1 of taurine by the high-spin Fe(IV) intermediate detected during oxygen activation by taurine:α-ketoglutarate dioxygenase (TauD), J. Am. Chem. Soc. 125 (2003) 13008–13009.